Desalination and Water Treatment
www.deswater.com

doi: 10.5004/dwt.2019.24408

163 (2019) 118–124
September

Evaluating the performance of extended and unscented Kalman filters in the reverse osmosis process

Seung Ji Lim[a], Seo Jin Ki[b,*], Jangwon Seo[a], Sung Ho Chae[a], Young Geun Lee[c], Kwanho Jeong[d], Jungsu Park[e], Joon Ha Kim[a]

[a]*School of Earth Sciences and Environmental Engineering, Gwangju Institute of Science and Technology (GIST), Gwangju 500-712, Korea*
[b]*Department of Environmental Engineering, Gyeongnam National University of Science and Technology, 33 Dongjin-ro, Jinju-si, Gyeongsangnam-do 52725, Republic of Korea, Tel. +82-55-751-3341; Fax: +82-55-751-3484; email: seojinki@gntech.ac.kr (S.J. Ki)*
[c]*Corporate R&D Institute, Doosan Heavy Industries & Construction Co. Ltd., Gyeonggi-do 16858, Korea*
[d]*Singapore Membrane Technology Centre, Nanyang Environment and Water Research Institute, Nanyang Technological University, Singapore 637141, Singapore*
[e]*Hanwha E&C (Engineering & Construction), 76, Gajeong-Ro, Yuseong-Gu, Daejeon 34128, Korea*

Received 9 February 2019; Accepted 14 May 2019

ABSTRACT

A Kalman filter (KF) algorithm is a recursive data processing algorithm typically recommended for estimating unmeasured state variables in chemical engineering processes. We studied the performance of a KF algorithm in a range of noise levels as well as indirectly observed data from the process model. For this study, two versions of the KF algorithm widely adopted for a nonlinear system, the extended Kalman filter and the unscented Kalman filter, were applied to 1-year time series data monitored during the operation of the Fujairah seawater reverse osmosis desalination plant. We found that variables indicating the state of fouling, membrane resistance, and solute permeability agreed well with those estimated by the two KF algorithms, specifically in terms of noise reduction and peak detection. When the two KF algorithms were exposed to various noise levels, they showed a corresponding increase in the error rates (for unmeasured state variables) according to the noise levels varying from 10% to 50%, regardless of the algorithms used. The two KF algorithms provided a good prediction performance only for the permeate flow rate rather than for the permeate concentration, out of the two types of measured data. However, the individual KF algorithms still showed different performances in computing estimated and predicted data in the reverse osmosis process. This result calls for further research on the determination of the best KF algorithms for either estimation or prediction of directly and indirectly measured state variables in various chemical processes.

Keywords: Seawater reverse osmosis (SWRO); Extended Kalman filter (EKF); Unscented Kalman filter (UKF); Noise reduction; Peak detection

1. Introduction

In response to high energy demands in the coming decades as well as cost-effective water production, seawater reverse osmosis (SWRO) plants must reduce their energy consumption [1,2]. Feed water disturbances, actuator and sensor failures, and membrane fouling were three major factors that affected energy usage in the SWRO process, when achieving desirable product water in terms of water quality and quantity under such conditions. Feed disturbances indicate short- (day or night) and long-term (seasonal change) variations of feed water sources (e.g., water temperature, total dissolved solid (TDS) concentration, and pH) [3], which has a significant effect on the permeate flow rate and permeate concentration. The SWRO process was found to also

* Corresponding author.

This article was originally published with errors on page 120 and the list of references. This version has been updated. Please see Corrigendum in vol. 270 (2022) 321 [doi: 10.5004/dwt.2022.29012].

be vulnerable to actuator and sensor failures (e.g., actuated pumps and valves), preventing the process from performing the expected operation, which, in turn, was likely to increase demand for energy use of the SWRO process. Membrane fouling describes the accumulation of particles during degraded filtration performance, which amplifies the energy consumption of the SWRO process over time, unless appropriate membrane cleaning or replacement are applied during the operation [4]. Therefore, accurate estimation of the process states using measured data plays an important role in lowering the energy consumption of the SWRO process.

Timely and accurate diagnosis of engineering process can be achieved using an observer, a computational algorithm that estimates the state and parameters of the process. In chemical and biochemical engineering systems, research on the design and implementation of the observer has been conducted in the past few decades. For example, many earlier studies have been dedicated to help adapt the observer in the chemical process. They mainly contain categorizations of observers and procedures to develop observers [5–7]. A Kalman filter (KF) is one of the most widely adopted observers among the previously developed observers. Although the KF was originally developed for a linear system [8], an extended version could be applied to a nonlinear system, especially chemical and biochemical engineering processes. The applied research fields of the KF algorithm cover a wide variety of topics, specifically including control and measurement engineering [7]. A good example of the KF in the chemical engineering process was to estimate the temperature for a counter-current heat exchanger [9]. Another example included control of the fermentation process that employed the KF to estimate indirectly measured biological variables [10,11]. Several previous studies often used the KF as fault detection and isolation method [12,13]. In conventional and advanced process control areas, the KF was also utilized in a data pre-processing step before the raw data were provided to the control module [14–16]. In those studies, reduction of noise or disturbance in input variables resulted in desirable system performance outcomes. In the fields of desalination research, an online estimator of fouling development was proposed using a non-linear recursive least-squares method, where the friction coefficient as well as membrane resistance were the main variables of interest [17].

In this study, we used the membrane resistance and solute permeability as indicators of the state of fouling, because the deterioration of membrane performance in the SWRO process could be indirectly described by these two parameters. Note that the membrane resistance and solute permeability play a role in predicting the permeate flow rate and concentration, although they are not measured directly with real-time sensors or laboratory experiments. Therefore, the aim of the present study was to determine the best KF algorithm for computing directly and indirectly measured variables with and without noise in an example time-series data set (of the Fujairah SWRO plant). Specifically, we used two non-linear KF algorithms, the extended Kalman filter (EKF) and the unscented Kalman filter (UKF), in calculating directly and indirectly observed variables in the SWRO process. The specific objectives of this study were (1) to assess the performance of the two KF algorithms in estimating state variables, (2) to test the stability of the two KF algorithms according to different noise levels, and (3) to compare the performance of the two KF algorithms in predicting measured data. We hope that the proposed methodology provides valuable insight into the best membrane cleaning and replacement schedule in the SWRO process from parameters monitored in real time.

2. Materials and methods

2.1. Test data sets in the pilot SWRO plant

Table 1 describes the characteristics of the major operational parameters observed (from real-time sensors) at the feed and permeate sides in the Fujairah SWRO plant during the 1-year monitoring period. As shown in the table, the Fujairah SWRO plant received raw seawater with temperatures ranging from 23°C to 37°C, and TDS concentrations ranging from 35,691 to 42,596 mg/L. After continuous treatment in the RO process, the TDS concentration at the permeate side was reduced significantly, but still varied between 362 and 823 mg/L, due to fluctuations in the feed water quality. The applied pressure at the feed side ranged from 65 to 73 bar depending on the raw water quality, which decreased to between 2 and 13 bar at the permeate side. Similarly, the flow rate at the feed site was maintained from 951 to 1,200 m^3/h, whereas the reverse osmosis (RO) process produced water with an average flow rate of 481 m^3/h. The recovery rate in the RO process was recorded at about 43% to 50% under the specific operating conditions of the feed side described above. Note

Table 1
Summary statistics of major input and output parameters observed during the 1-year monitoring period at the Fujairah SWRO plant

Locations	Parameters	*N*	Range	Mean
Feed side	Temperature (T_f), °C	365	23–37	29
	TDS concentration (C_f), mg/L	365	35,691–42,596	38,829
	Flow rate (Q_f), m^3/h	365	951–1,200	1,119
	Pressure (P_f), bar	365	65–73	67
Permeate side	TDS concentration (C_p), mg/L	365	362–823	495
	Flow rate (Q_p), m^3/h	365	448–516	481
	Recovery, %	365	43–50	45
	Pressure (P_p), bar	365	2–13	10

TDS = Total dissolved solids

that all recorded data contain some noise associated with the sensor measurements. Thus, those data are processed to reduce the inherent noise in the data set as well as to predict important parameters that should be maintained either above or below the designated value using two types of Kalman filter algorithms, as described in Sections 2.2–2.4.

It is noted that the observed data of Fujairah plant described in this section was previously used to conduct numerical studies of the reverse osmosis process [17–19]. The same data was employed to evaluate the performance of two Kalman filter algorithms for estimating fouling in the reverse osmosis process.

2.2. Reverse osmosis process model

Typically, water flux and salt flux are used to assess the performance of the RO membrane. This is because those two types of flux are found to be decreased or increased progres-sively according to the accumulation of foulants. Among various models available in literature, we adopted the solution–diffusion model, a popular model in non-porous polymer membranes, to estimate the water flux and salt flux in the RO membrane. According to the solution–diffusion model, the water flux and salt flux are expressed as follows:

$$J_w = A \times \left(\Delta P - \Delta\pi\right) \tag{1}$$

$$J_s = B \times \left(C_f - C_p\right) = B \times \Delta C \tag{2}$$

where J_w and J_s indicate the water flux and salt flux, respectively [20]. In particular, J_w is proportional to the difference between transmembrane pressure ΔP and osmotic pressure difference $\Delta\pi$. The equation for the water flux is then developed by multiplying water permeability A by the difference between ΔP and $\Delta\pi$. In a similar manner, J_s is calculated by multiplying salt permeability B by the concentration difference between the feed and permeate water ΔC. Permeate flow rate Q_p and permeate concentration C_p can be calculated by using Eqs. (1) and (2):

$$Q_p = J_w \times W \times L \times \text{Ele} \times PV = A \times \left(\Delta P - \Delta\pi\right) \times W \times L \times \text{Ele} \times PV \tag{3}$$

$$C_p = \frac{J_s}{J_w} = \frac{B \times \Delta C}{A \times \left(\Delta P - \Delta\pi\right)} \tag{4}$$

where W and L are the width and length of the RO membrane, respectively. Ele is the number of elements in a pressure vessel. PV indicates the number of pressure vessels employed in the RO plant.

2.3. System model for Kalman filter algorithms

The dynamics of foulants on the RO membrane can be expressed using the theory of transport phenomena. The total amount of foulants M accumulated in the membrane with respect to time t can be expressed as follows:

$$M = \int_0^t J_f \, dt = C_{f0} \int_0^t v \, dt \tag{5}$$

where J_f is the rate of deposition of the foulants. C_{f0} and v are the bulk foulants concentration and permeate velocity, respectively. The amount of deposited foulants is assumed to increase with the membrane resistance in a linear fashion:

$$\Delta R_a = r_s M = r_s C_{f0} \int_0^t v \, dt = k_{fp} \int_0^t v \, dt \tag{6}$$

where ΔR_a indicates the increase in the membrane resistance depending on the fouling accumulation [21]. r_s is the specific resistance of the fouling layer. k_{fp} is the fouling potential coefficient, indicating the possibility of fouling in the feed water. If the state of fouling (SOF) is described by the membrane resistance, the total membrane resistance can be given by the following equations:

$$R_t = R_m + \Delta R_a \tag{7}$$

$$\Delta R_a = k_{\text{fp}} \int_0^t v\left(\tau\right) d\tau \tag{8}$$

where R_m is the intrinsic membrane resistance [19]. From the principle of membrane transfer, membrane resistance R_t is estimated by the reciprocal of water permeability A. The permeate velocity can be calculated using Eqs. (1) and (7). By differentiating each side of Eq. (6), the first equation for the SOF can be derived:

$$v = \frac{\Delta P - \Delta\pi}{R_t} \tag{9}$$

$$\frac{dR_t}{dt} = k_{\text{fp}} v = k_{\text{fp}} \frac{\Delta P - \Delta\pi}{R_t} \tag{10}$$

Rearrangement of Eq. (2) gives the following form of the equation to calculate salt permeability B:

$$B = C_p \times \frac{A\left(\Delta P - \Delta\pi\right)}{C_f - C_p} = \frac{C_p}{C_f} \times \frac{A\left(\Delta P - \Delta\pi\right)}{1 - \dfrac{C_p}{C_f}} = \frac{1-r}{r} \times \frac{\Delta P - \Delta\pi}{R_t} \tag{11}$$

where $(r = 1 - C_p/C_f)$ is the rejection rate of the RO membrane. If we set r at 0.995 and assume the difference between ΔP and $\Delta\pi$ is constant, the differentiation of Eq. (10) gives the second form of the equation for the SOF:

$$\frac{dB}{dt} = -k_{\text{fp}} \times \frac{1-r}{r} \times \frac{\left(\Delta P - \Delta\pi\right)^2}{\left(R_t\right)^3} \tag{12}$$

Note that the total membrane resistance and solute permeability, which are not measured using real-time sensors, are state variables to be estimated using two types of Kalman filter algorithms.

2.4. Kalman filter algorithms for a nonlinear system

In this study, two types of Kalman filter algorithms are used to estimate the membrane resistance and solute

permeability in the RO process model, and to predict the permeate flow rate and concentration. The KF is a recursive data processing algorithm developed for a linear system, but the algorithm can also be extended to a nonlinear system after linearization of the process. Two popular variants developed for a nonlinear system are the EKF and UKF algorithms. It is assumed in all KF algorithms that the process and measurement noises are characterized by independent, zero-mean, and Gaussian noise.

The EKF algorithm searches the best weights for model prediction and measurement. Estimations of the state variables and statistical weights are computed using the following equations [5,8]:

$$\hat{x}_t^- = f\left(\hat{x}_{t-1}\right) \tag{13}$$

$$P_t^- = AP_{t-1}A^T + Q \tag{14}$$

$$K_t = P_t^- H^T \left(HP_t^- H^T + R\right)^{-1} \tag{15}$$

$$\hat{x}_t = \hat{x}_t^- + K_t\left(z_t - h\left(\hat{x}_t^-\right)\right) \tag{16}$$

$$P_t = P_t^- - K_t H P_t^- \tag{17}$$

where x is a matrix of the state variables. The calculated values of the membrane resistance and salt permeability using plant operational data are assigned as elements of matrix z. The membrane resistance and salt permeability can be calculated by using Eqs. (9) and (11), respectively:

$$x_t = \begin{bmatrix} R_t \\ B \end{bmatrix} \tag{18}$$

$$z_t = \begin{bmatrix} R_t \\ B \end{bmatrix} \tag{19}$$

f is the discrete form of the system model in Eqs. (6) and (7). P_t is the error covariance. A is a Jacobian of the system model:

$$A = \begin{bmatrix} -k_{\text{fp}} \dfrac{\Delta P - \Delta\pi}{R_t^2} & 0 \\ 0 & 3 \times k_{\text{fp}} \times \dfrac{1-r}{r} \times \dfrac{\left(\Delta P - \Delta\pi\right)^2}{\left(R_t\right)^4} \end{bmatrix} \tag{20}$$

Q and R are the error covariance matrix of the noise for the system model and measurements, respectively:

$$Q = \begin{bmatrix} 10^{11} & 0 \\ 0 & 0.3 \end{bmatrix} \tag{21}$$

$$R = \begin{bmatrix} 10^{11} & 0 \\ 0 & 0.3 \end{bmatrix} \tag{22}$$

K_t is the Kalman gain. H is a matrix describing the relation between the measurements and state variables:

$$H = \begin{bmatrix} 1 & 0 \\ 0 & 1 \end{bmatrix} \tag{23}$$

Eqs. (13)–(17) require two-phase computation, the prediction and correction steps. In the prediction step, Eqs. (13) and (14) are used to predict the system variables. In the correction step, Eqs. (15) and (16) calculate the statistical weights, including an estimation of the system variables. Eq. (17) is employed to update the error covariance in the next time step.

The UKF algorithm adopts more enhanced statistical analysis than the EKF algorithm. The EKF algorithm estimates the Jacobian A of the system model during the process of updating the covariance, whereas the UKF algorithm does not require it. Instead, the UKF algorithm conducts sampling of the sigma point and performs the unscented transformation. The detailed algorithms embedded in the UKF algorithm are as follows:

$$\left(\chi_i, W_i\right) \leftarrow \left(\hat{x}_{t-1}, P_{t-1}, \kappa\right) \tag{24}$$

$$\left(\hat{x}_t^-, P_t^-\right) = \text{UT}\left(f\left(\chi_i\right), W_i, Q\right) \tag{25}$$

$$\left(\hat{z}_t, P_z\right) = \text{UT}\left(h\left(\chi_i\right), W_i, R\right) \tag{26}$$

$$P_{xz} = \sum_{i=1}^{2n+1} W_i \left\{f\left(\chi_i\right) - \hat{x}_t^-\right\}\left\{h\left(\chi_i\right) - \hat{z}_t\right\}^T \tag{27}$$

$$K_t = P_{xz} P_z^- \tag{28}$$

$$\hat{x}_t = \hat{x}_t^- + K_t\left(z_t - \hat{z}_t\right) \tag{29}$$

$$P_t = P_t^- - K_t P_z K_t^T \tag{30}$$

where χ is the sigma point, and W is the weight required to compute the covariance and the average. UT is an abbreviation for unscented transformation. Note that the computation process of the UKF algorithm is identical to that of the EKF algorithm, except for the adopted equations in individual algorithms. Eqs. (24)–(27) are used for the prediction process, whereas Eqs. (28)–(30) are adopted in the calibration process. More detailed information about the EKF and UKF algorithms are also available in literature [8,20].

3. Results and discussion

The numerical simulations were conducted (1) to evaluate the performance of the two KF algorithms in estimating state variables, (2) to test the stability of the two KF algorithms according to different noise levels, and (3) to compare the prediction performance of the two

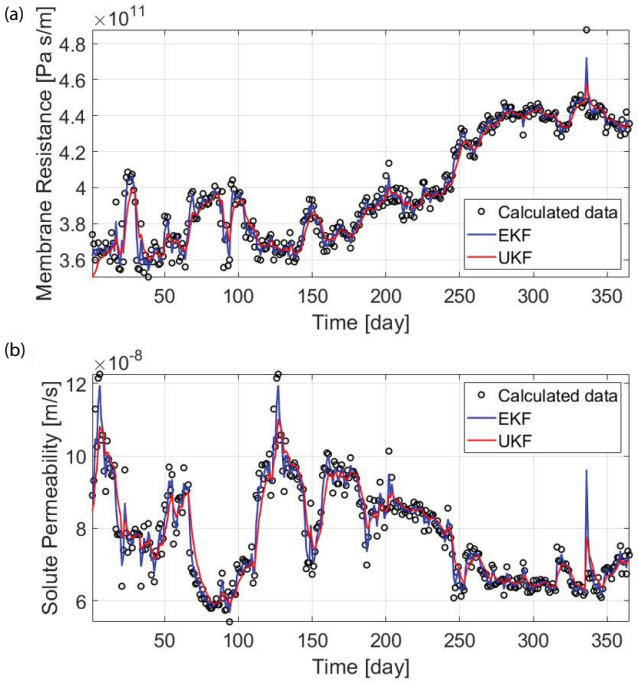

Fig. 1. An estimation of (a) the membrane resistance and (b) solute permeability during the 1-year monitoring period using two types of Kalman filter algorithms, the EKF (see the solid blue line) and UKF algorithms (see the solid red line).

KF algorithms in predicting the permeate flow rate and permeate concentration. The second scenario was designed to simulate sensor failure during the operation of a real plant. Sensor failure can increase the noise in the measured data, affecting the estimation of indirectly monitored variables. Noise was generated by using a random number generator. Simulation data with different noise levels were generated by adding noise to the membrane resistance and salt permeability data calculated from Eqs. (9) and (11), respectively. The estimated state variables using the two KF algorithms were applied to Eqs. (3) and (4), to calculate the permeate flow rate and permeate concentration. The permeate flow rate and permeate concentration were measured by the sensor, and compared with the calculated values. The simulation conditions used in the system model of the KF algorithms were determined based on the initial design of the Fujairah plant provided in the studies by Lee et al. [18] and Sanza et al. [23]. Those parameter values are presented in Table 2.

3.1. Estimation of indirectly observed data using two types of KF algorithms

Figs. 1a and b illustrate the membrane resistance and solute permeability estimated by two types of KF algorithms, respectively. Note that the membrane resistance and solute permeability are indirectly computed from the principle of membrane transfer and Eq. (11), using operating data from the pilot plant. In Fig. 1a, the membrane resistance exhibits two distinct patterns during the 1-year monitoring period. In other words, the membrane resistance fluctuated slightly between 3.5 and 4.1 × 10^{11} Pa·s/m for 160 d. However, a sudden increase in the membrane resistance reaching as high as around 4.9 × 10^{11} Pa·s/m, was observed during the remaining monitoring period. This indicated that membrane fouling occurred progressively during the operation of the RO process. The EKF and UKF algorithms did not always under- and over-estimate the membrane resistance, and showed excellent agreement with the observed data, excluding one case that displayed a sharp increase in the membrane resistance at around 340 d. In contrast, the solute permeability fluctuated considerably, between 6.0 × 10^{-8} and 12.0 × 10^{-8} m/s, without an obvious trend until 160 d, and then decreased constantly after that, as opposed to that of the membrane resistance. Both algorithms successfully estimated the solute permeability, but seemed to show large deviations from the indirectly estimated data, compared with that of the membrane resistance. Of the two algorithms, the UKF algorithm had superior performance compared with the EKF algorithm in terms of noise reduction, although both successfully detected the peaks of the membrane resistance and solute permeability.

Table 2
Parameter values used in the system model assessment

Parameters	Values
Length of RO membrane, L (m)	1
Width of RO membrane, W (m)	37
Number of elements in a pressure vessel, Ele (ea)	7
Number of pressure vessels, PV	136
Solute rejection rate, r (-)	0.995
Membrane intrinsic resistance, R_m (Pa s/m)	3.5 × 10^{11}
Fouling potential coefficient (Pa s/m^2)	3.5 × 10^9
Total number of days	365

3.2. Tolerance of two types of KF algorithms against noise levels in the data set

Fig. 2 presents the performance of the EKF algorithm and UKF algorithm in terms of error rates, according to increased noise levels of the membrane resistance and solute permeability from 10% to 50%. It was determined from Figs. 2a and b that the error rates of the membrane resistance computed from the two algorithms increased steadily with increasing noise levels. However, the EKF algorithm displayed a larger increase in error rates than the UKF algorithm, reaching as high as around 30% (except for outliers) when the noise levels in the membrane resistance increased up to 50%. Interestingly, the interquartile range box containing the middle 50% of the data was quite small for the UKF algorithm, compared with that of the EKF algorithm. However, the UKF algorithm still produced numerous outliers exceeding a few standard deviations, regardless of the noise levels added intentionally (see the red plus symbol). The error rates of the solute permeability estimated from both algorithms showed almost identical patterns as for those of the membrane resistance, but with slightly increased error rates in response to the noise levels (compare

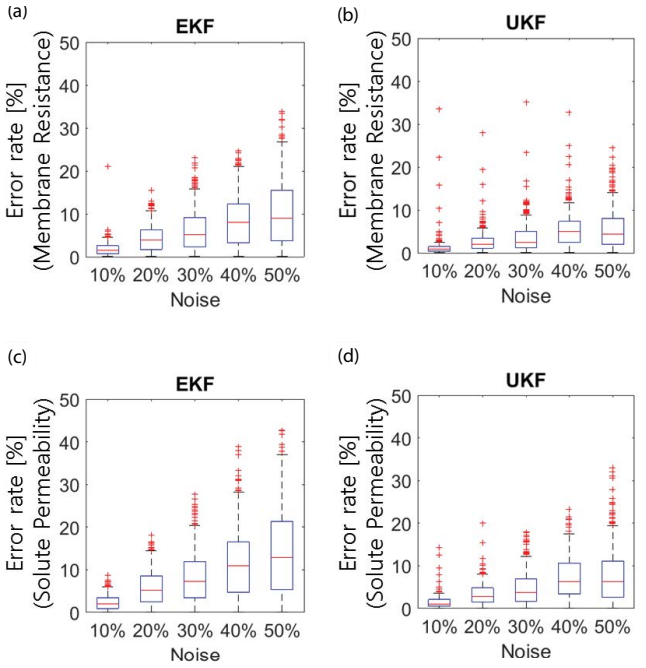

Fig. 2. Estimated error rates of the membrane resistance and solute permeability in the EKF and UKF algorithms in response to an increase in the data noise from 10% to 50%.

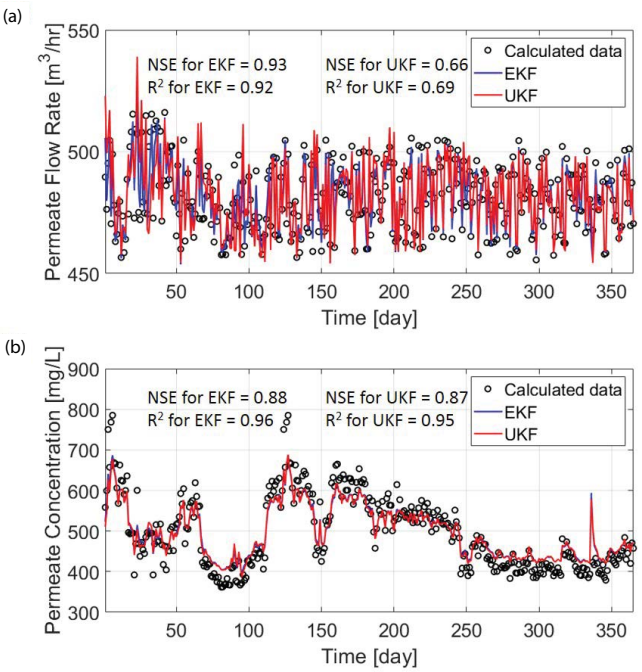

Fig. 3. Prediction results of (a) the permeate flow rate and (b) permeate concentration implemented in the RO process model using the EKF (see the solid blue line) and UKF algorithms (see the solid red line) during the 1-year monitoring period.

the lengths of the box spanning the interquartile range in the error rates for both parameters). The error rates of the solute permeability rose by 40% for the EKF algorithm and 20% for the UKF algorithm (except for outliers) at the 50% noise level. In addition, many outliers exceeding a few standard deviations were not observed when estimating the solute permeability from the UKF algorithm under various noise levels, unlike the membrane resistance. These results implied that the UKF algorithm was less sensitive to the noise levels in the data set than the EKF algorithm, but had the potential to produce many outliers, even at low noise levels, depending on the magnitude of parameter of interest. Of course, the error rates computed from the two algorithms increased with increasing noise levels.

3.3. Prediction of directly measured data using two types of KF algorithms

We also evaluated the performance of the two algorithms in predicting directly observed data, the permeate flow rate and concentration (Figs. 3a and b). Note that the permeate flow rate and concentration were measured directly by sensors in the permeate side at discrete time intervals (see the back open circle), whereas the corresponding parameters were also predicted by applying both algorithms (see the solid blue and red lines) to Eq. (3) (for the permeate flow rate) and Eq. (4) (for the permeate concentration). Fig. 3a shows that there is a significant difference in the predicted permeate flow rate between the two algorithms. The performance of the EKF algorithm was superior to that of the UKF algorithm in terms of Nash–Sutcliffe efficiency (NSE) and R^2. However, the EKF algorithm often slightly overestimated the permeate flow rate of the RO process in different periods of (operation) time. The EKF and UKF algorithms did not correctly compute the permeate concentration (see NSE and R^2). The pattern of the permeate concentration predicted by the EKF algorithm was almost identical to that of the UKF algorithm, including a case that showed an abrupt increase in the permeate concentration at around 340 d. These results revealed that the performance of both algorithms was quite comparable, although the EKF algorithm showed a slightly improved performance in predicting a particular operating parameter during the operating period of the pilot RO plant. However, we cannot provide a clear explanation for the difference in the performance of the two algorithms in computing indirectly and directly measured data at this moment.

4. Conclusions

This study was designed to assess the performance of KF algorithms in computing directly and indirectly observed data in the absence and presence of noise in the data set. The operating data in an SWRO desalination process over a 1-year monitoring period was used as the test data set to which two types of KF algorithms, the EKF and the UKF, were applied. From this study, we obtained the following conclusions.

- The EKF and UKF algorithms successfully estimated indirectly observed state variables, the membrane resistance and solute permeability, with respect to noise reduction and peak detection. Although the two versions of KF algorithms showed similar performances, the UKF algorithm seemed better able to reduce noise in the data, specifically for parameters varying over larger orders of magnitude.

- The EKF and UKF algorithms did not resist well noise imposed at different levels. The error rates of the membrane resistance and solute permeability increased progressively in response to increase in the noise levels from 10% to 50%. The EKF algorithm appeared to yield larger error rates than the UKF algorithm, but produced fewer outliers that were far beyond a few standard deviations than the UKF algorithm.
- The prediction performance of directly measured data using the two KF algorithms was slightly different from that of indirectly observed data. Although the algorithms showed a similar performance in predicting directly measured data, the permeate flow rate and concentration, the EKF algorithm recorded a slightly higher prediction accuracy for the permeate flow rate than the UKF algorithm. Further research is still warranted to clearly address the inconsistent performance of two versions of KF algorithms for directly and indirectly observed variables in the RO process.

Acknowledgments

This work was supported by the Korea Environment Industry & Technology Institute (KEITI) through the Industrial Facilities & Infrastructure Research Program, funded by Korea Ministry of Environment (MOE) (grant RE201901121). In addition, we would like to thank Doosan Heavy Industries & Construction for providing experimental data from the Fujairah plant in United Arab Emirates.

Symbols

Reverse osmosis model

A — Water transport coefficient, m/(s Pa)
B — Salt transport coefficient, m/s
J_w — Water flux, m/s
J_s — Solute flux, kg/m^2 s
Q — Flow rate, m^3/h
P — Pressure, Pa
p — Osmotic pressure, Pa
C — TDS concentration, mg/L
V — Permeate velocity
T — Time, d
M — Total amount of foulants deposited on the membrane, mg/m^2
J_f — Rate of foulants deposition, mg/m^2 s
C_{f0} — Bulk foulants concentration, mg/L
r_s — Specific resistance of the fouling layer, Pa m s/g
R_m — Intrinsic membrane resistance, Pa s/m
R_a — Membrane resistance due to accumulation of foulants, Pa s/m
R_t — Total membrane resistance, Pa s/m
k_{fp} — Fouling potential coefficient, Pa s/m^2

Kalman filter

x — Matrix of the state variable
z — Matrix for observed data
f — Discrete form of the system model
P — Error covariance
A — Jacobian of the system model
Q — Error covariance matrix of noise for the system model
R — Error covariance matrix of noise for measurement
K — Kalman gain
H — Matrix for the relation between the measurements and the state variables

References

[1] G.-R. Xu, J.-N. Wang, C.-J. Li, Strategies for improving the performance of the polyamide thin film composite (PA-TFC) reverse osmosis (RO) membranes: surface modifications and nanoparticles incorporations, Desalination, 328 (2013) 83–100.
[2] J. Xu, Z. Wang, L. Yu, J. Wang, S. Wang, A novel reverse osmosis membrane with regenerable anti-biofouling and chlorine resistant properties, J. Membr. Sci., 435 (2013) 80–91.
[3] C.W. McFall, A. Bartman, P.D. Christofides, Y. Cohen, Control and monitoring of a high recovery reverse osmosis desalination process, Ind. Eng. Chem. Res., 47 (2008) 6698–6710.
[4] C. Fritzmann, J. Löwenberg, T. Wintgens, T. Melin, State-of-the-art of reverse osmosis desalination, Desalination, 216 (2007) 1–76.
[5] D. Dochain, State and parameter estimation in chemical and biochemical processes: a tutorial, J. Process Control, 13 (2003) 801–818.
[6] J. Prakash, R.B. Gopaluni, S.C. Patwardhan, S. Narasimhan, S.L. Shah, Nonlinear Bayesian State Estimation: Review and Recent Trends, 2011 International Symposium on Advanced Control of Industrial Processes (ADCONIP), 2011, pp. 450–455.
[7] J. Mohd Ali, N. Ha Hoang, M.A. Hussain, D. Dochain, Review and classification of recent observers applied in chemical process systems, Comput. Chem. Eng., 76 (2015) 27–41.
[8] G. Welch, G. Bishop, An Introduction to the Kalman Filter, University of North Carolina at Chapel Hill, 1995.
[9] F. Bagui, M.A. Abdelghani-Idrissi, H. Chafouk, Heat exchanger Kalman filtering with process dynamic acknowledgement, Comput. Chem. Eng., 28 (2004) 1465–1473.
[10] W. Liu, An extended Kalman filter and neural network cascade fault diagnosis strategy for the glutamic acid fermentation process, Artif. Intell. Eng., 13 (1999) 131–140.
[11] J. Wang, L. Zhao, T. Yu, On-line Estimation in fed-batch fermentation process using state space model and unscented Kalman filter, Chin. J. Chem. Eng., 18 (2010) 258–264.
[12] L.A. Aguirre, M.F.S. Pereira, A modified observer scheme for fault detection and isolation applied to a poorly observed process with integration, J. Process Control, 8 (1998) 47–56.
[13] Z. Wang, H. Shang, Kalman filter based fault detection for two-dimensional systems, J. Process Control, 28 (2015) 83–94.
[14] J.H. Lee, N.L. Ricker, Extended Kalman Filter Based Nonlinear Model Predictive Control, 1993 American Control Conference, 1993, pp. 1895–1899.
[15] J.H. Lee, N.L. Ricker, Extended Kalman filter based nonlinear model predictive control, Ind. Eng. Chem. Res., 33 (1994) 1530–1541.
[16] S.-M. Ahn, M.-J. Park, H.-K. Rhee, Extended Kalman filter-based nonlinear model predictive control for a continuous MMA polymerization reactor, Ind. Eng. Chem. Res., 38 (1999) 3942–3949.
[17] D.Y. Kim, M.H. Lee, S. Lee, J.H. Kim, D.R. Yang, Online estimation of fouling development for SWRO system using real data, Desalination, 247 (2009) 200–209.
[18] Y.G. Lee, Y.S. Lee, D.Y. Kim, M. Park, D.R. Yang, J.H. Kim, A fouling model for simulating long-term performance of SWRO desalination process, J. Membr. Sci., 401–402 (2012) 282–291.
[19] S.J. Lim, Y.M. Kim, H.S. Park, S.J. Ki, K. Jeong, J. Seo, S.H. Chae, J.H. Kim, Enhancing accuracy of membrane fouling prediction using hybrid machine learning models, Desal. Water Treat., 146 (2019) 22–28.
[20] J.G. Wijmans, R.W. Baker, The solution–diffusion model: a review, J. Membr. Sci., 107 (1995) 1–21.
[21] K.L. Chen, L. Song, S.L. Ong, W.J. Ng, The development of membrane fouling in full-scale RO processes, J. Membr. Sci., 232 (2004) 63–72.
[22] E.A. Wan, R.V.D. Merwe, The Unscented Kalman Filter for Nonlinear Estimation, Proc. IEEE 2000 Adaptive Systems for Signal Processing, Communications, and Control Symposium (Cat. No. 00EX373), 2000, pp. 153–158.
[23] M.A. Sanza, V. Bonnélyea, G. Cremerb, Fujairah reverse osmosis plant: 2 years of operation, Desalination, 203 (2007) 91–99.